ORMOLYTEs (ORganically MOdified ceramic electroLYTEs): Solid State Protonic Conductors by the Sol–Gel Process

H. Schmidt,[a] M. Popall,[a] F. Rousseau,[a,b]
C. Poinsignon,[b] M. Armand[b] & J. Y. Sanchez[b]

[a] Fraunhofer-Institut für Silicatforschung, Neunerplatz 2, D-8700 Würzburg, FRG
[b] Laboratoire d'Ionique et d'Electrochimie du Solide de Grenoble, ENSEEG, BP 75, 38402 St Martin d'Hères Cedex, France

ABSTRACT

Protonic conductive polymers have been synthesized by the sol–gel process. the materials are obtained by hydrolysis and condensation of amino alkyl trimethoxysilane, with dissolved CF_3SO_3H as proton donor. The influence of the alkylamine chain on hydrolysis and condensation and on the properties of the final material has been studied. These materials are obtained in the form of transparent films, which are amorphous, hard and non-porous, with densities around 1·3 g cm^{-3}. The materials are stable in air up to 220°C. The ionic conductivity reaches from about 3×10^{-5} Ω^{-1} cm^{-1} at room temperature to about 10^{-2} Ω^{-1} cm^{-1} at 120°C with a 1·2 V stability window.

INTRODUCTION

The main drawback of ionic conductive polymers such as PEO complexes is the formation of crystalline phases at room temperature, leading to a conductivity decrease.[1] Ravaine *et al.*[2] and Charbouillot[3] have shown the possibility of obtaining amorphous solvating polymers

by using the sol–gel route. Moreover the sol–gel process presents special advantages in comparison to conventional processing techniques:[4] besides high reactivity, homogeneity and purity of the precursors, it allows special shaping techniques such as coating films or powder formation.

A suitable route to sol–gel materials is the hydrolysis and the condensation of alkoxides, e.g. $Si(OR)_4$ or $R'_nSi(OR)_{4-n}$, R′ representing an organofunctional grouping and R an alkyl group. The hydrolysis and the condensation of $R'_nSi(OR)_{4-n}$ can be schematically described by eqns (1)–(3):

Hydrolysis:

$$\equiv Si{-}OR + H_2O \rightleftharpoons \equiv Si{-}OH + ROH \qquad (1)$$

Condensation:

$$\equiv Si{-}OH + RO{-}Si\equiv \rightleftharpoons \equiv Si{-}O{-}Si\equiv + ROH \qquad (2)$$

$$\equiv Si{-}OH + HO{-}Si\equiv \rightleftharpoons \equiv Si{-}O{-}Si\equiv + H_2O \qquad (3)$$

Condensates with one non-hydrolysable ligand can be described by a silicate network with functional organic substituents R′ (Fig. 1). The inorganic backbone provides mechanical strength and an amorphous structure at room temperature. Organic groups can provide solvating properties to ionic compounds (acids, salts).

In this study the influence of the organofunctional grouping on the hydrolysis and condensation reactions will be shown and resulting material properties are investigated. The understanding of hydrolysis and condensation is necessary to control structure and properties of the material.

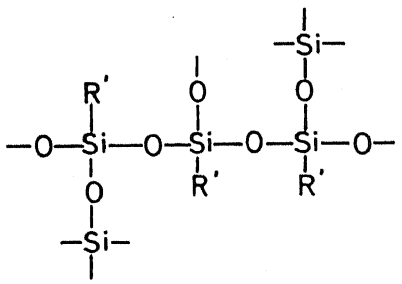

Figure 1. Possible ORMOLYTE structure by sol–gel process.

EXPERIMENTAL

The materials are synthesized by mixing at room temperature H_2O, CH_3OH and $(CH_3O)_3SiR'$ in a 1·5 : 9·5 : 1·0 molar ratio. The solution is stirred for 5 h and CF_3SO_3H is added as a proton donor before removing the excess of solvent by evaporation. The viscous solution obtained is cast on a Teflon plate and dried at 50°C. Gelation with minimum of shrinkage or cracking takes place rapidly during drying. In order to determine the influence of the organic group on hydrolysis and condensation, three variations of $(CH_3O)_3SiR'$ as precursor have been used:

$$\text{amo:} \quad R' = (CH_2)_3NH_2;$$

$$\text{diamo:} \quad R' = (CH_2)_3NH(CH_2)_2NH_2$$

$$\text{triamo:} \quad R' = (CH_2)_3NH(CH_2)_2NH(CH_2)_2NH_2.$$

The CF_3SO_3H concentration is expressed as the molar ratio x of CF_3SO_3H to the total amount of available amino nitrogen, $[CF_3SO_3H]:[N]$. x has been varied between 0 and 0·3.

Kinetic measurements (gas chromatography, water titration by Karl Fischer method, FT–IR spectroscopy) have been performed by analysing the reaction solution (same conditions were used as for the synthesis). Gas chromatography (Carbowax 1500 column for methanol and an AK 30 000 column by Perkin Elmer for silanes) was used for monitoring the changes of the concentrations of methanol and monomer during the hydrolysis and condensation process. FT–IR spectroscopy has been carried out with the circle cell equipment (multiple internal reflection device) using a ZnSe crystal. The thermochemical behaviour has been investigated by differential thermal analysis and differential gravimetric analysis coupled with mass spectrometry using a heating rate of $10\,K\,min^{-1}$. To obtain information about the amorphous or crystalline character of the materials X-ray diffraction analysis has been performed at room temperature.

AC complex impedance spectroscopy was used to measure the ionic conductivity of the samples. Flat samples are covered on both sides with a conductive graphite suspension and dried under vacuum at 120°C for 24 h in order to remove the absorbed carbon dioxide and water. The stability window was determined using three-electrode cyclic voltammetry, with a powderized platinum working electrode (area about 7 mm^2), a hydrogenated Ti–Ni alloy electrode as reference

and a stainless steel counter electrode. The experiments were carried out under vacuum at 100°C by starting on the cathodic side.

RESULTS AND DISCUSSION

Hydrolysis and Condensation Reaction

As shown for amo on Fig. 2 the water disappearance occurs with a nearly total depletion of the monomer within 15 min, indicating the catalytic effect of the amino groupings on the hydrolysis. Gas chromatography can only detect unhydrolysed monomers. After the unhydrolysed monomer has disappeared, hydrolysis still pro-

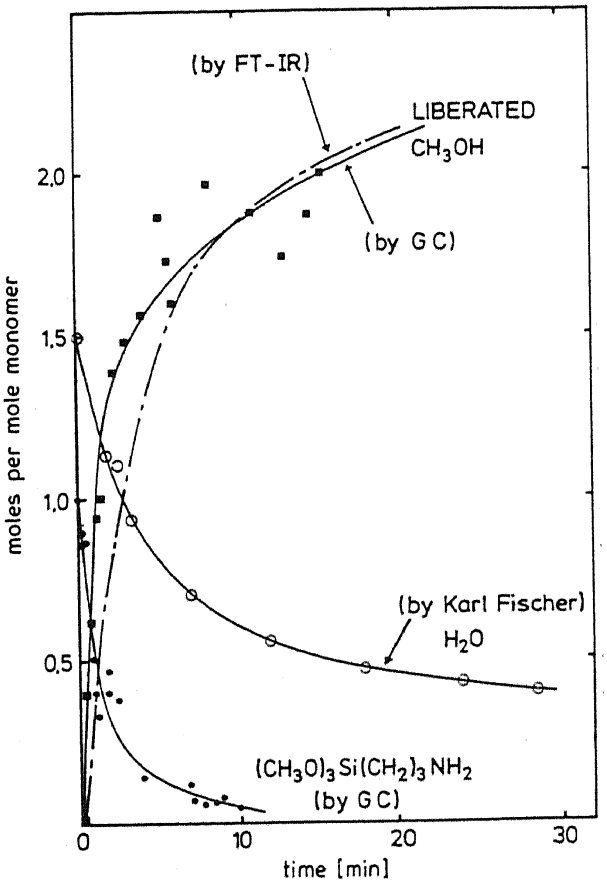

Figure 2. Hydrolysis of amo.

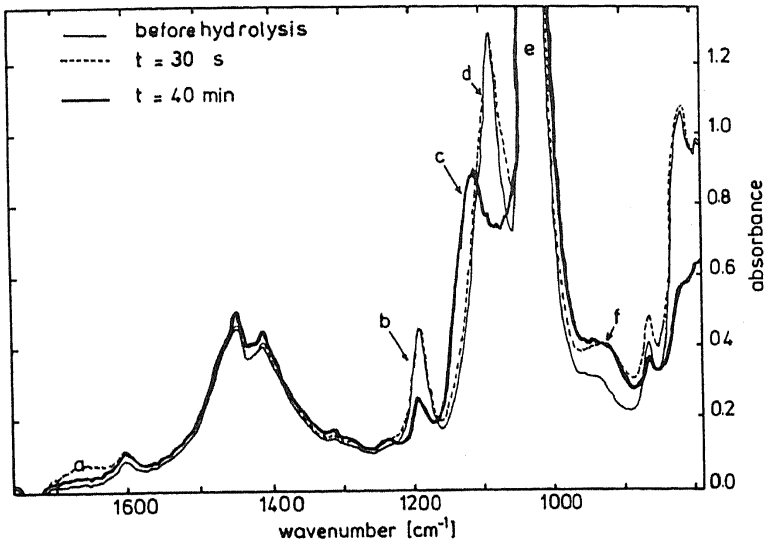

Figure 3. The FT–IR absorbance spectra of the amo system: before, 30 s and 40 min after water addition. Deformation of molecular water: peak (a) around 1650 cm^{-1}; Si—OCH_3 rocking and stretching vibrations: peaks (b) at 1190 cm^{-1} and (d) at 1080 cm^{-1}; Si—O—Si stretching vibration: peak (c) at 1130 cm^{-1}. Another peak at 1040 cm^{-1} corresponding to the silicate network, too, is superposed by the peak (e) (C—O stretching of methanol). The shoulder (f) at 950 cm^{-1} (SiO^- SiOH stretching[14]) indicates the formation of silanols groups.

ceeds by hydrolysing mixed monomers ($HO(CH_3O)_2SiR'$ or $(HO)_2(OCH_3)SiR'$) or oligomers already formed.

The evolution of CH_3OH can be determined by gas chromatography as well as indirectly calculated by the disappearance of the Si—OCH_3 bond in the FT–IR spectrum (Fig. 3). The two curves in Fig. 2 do not match completely, probably due to the higher experimental error of the gas chromatography. The ratio of the H_2O decay to the evolution of CH_3OH, which is close to two, indicates an almost complete condensation immediately after hydrolysis. Continuous evaluation of the type of peaks indicated in Fig. 3 is shown in Fig. 4 for amo compared to triamo. It confirms the findings of Fig. 2 for amo, that the formation of SiOSi bonds (≡ condensation) starts at a very early stage of the reaction. The low concentration of SiOH groups within the first 60 min supports the interpretation that SiOH groups formed either condense by reaction (2) or (3) immediately after formation. Figure 4 shows clear differences between amo and triamo. Together with the H_2O consumption and CH_3OH deliberation kinetics in Fig. 5, the

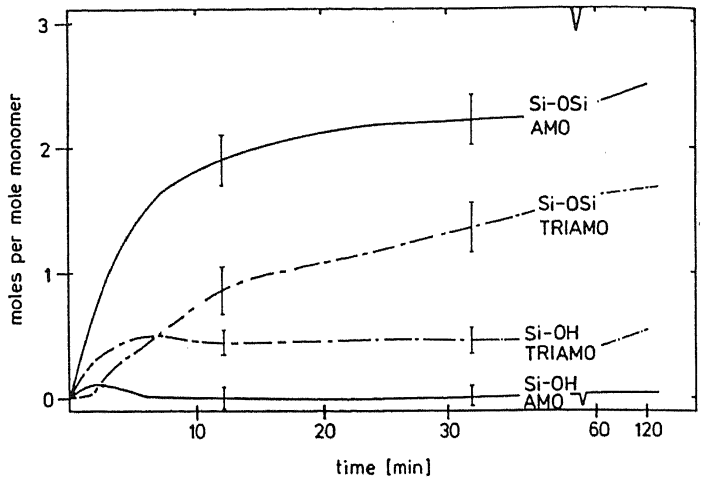

Figure 4. Formation of SiOH and SiOSi for amo and triamo by hydrolysis and condensation; FT–IT data.

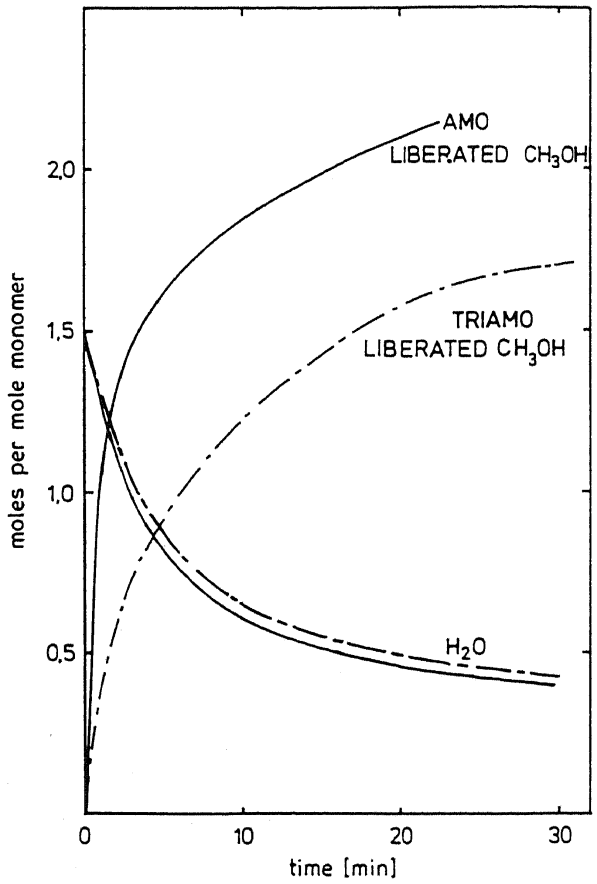

Figure 5. H_2O consumption and CH_3OH formation for amo and triamo; CH_3OH determined by GC; H_2O determined by Karl Fischer titration; ——, amo; · — · — ·, triamo.

differences can be explained as follows. In the case of triamo, about 0·5 mol ≡SiOH/Si are measured after 10 min reaction time, corresponding approximately to the difference of 0·5 mol of CH_3OH compared to amo (Fig. 5) and in accordance with a remarkably lower concentration of SiOSi bonds at this time. After 10 min the ≡SiOH concentration reaches a constant level (both for amo and triamo). Hydrolysis and condensation are related by (4)–(6)

$$[\equiv SiOR] + [H_2O] \rightarrow [\equiv SiOH] + [HOR] \quad (4)$$

$$[\equiv SiOH] + [ROSi] \rightarrow [\equiv SiOSi\equiv] + [HOR] \quad (5)$$

$$\text{or } 2\ [\equiv SiOH] \rightarrow [\equiv SiOSi\equiv] + [H_2O] \quad (6)$$

((6) does not change the overall balance). For c_{SiOH} = constant the formation of ≡SiOSi≡ is linear proportional to the decay of c_{H_2O}. Since the H_2O consumption rate for amo and triamo are the same (Fig. 5), the ≡SiOSi≡ formation rate (condensation rate) has to be the same for amo and triamo, too, in the c_{SiOH} = constant region. From 0 to 10 min the condensation rate is higher for amo as one can see from Fig. 4. After 60 min the SiOH concentrations are increasing slightly, probably due to the fact that stiff oligomers are formed by time with SiOH groups sterically hindered from condensation. Amo and triamo are both hydrolysing fast at the beginning of the reaction. While amo immediately starts condensation, the condensation reaction of triamo is slower, thus producing higher concentrations of ≡SiOH. The reason of this may lay in an increasing steric hindrance by the $—(CH_2)_3NH(CH_2)_2NH(CH_2)_2NH_2$ chain or even in a weak internal coordination of the $—NH_2$ group to the Si, thus blocking a reactive site.[5] With increasing SiOH concentration the condensation rate increases too, reaching a constant level. Whether the condensation occurs via (2) or (3) cannot be distinguished by this experiment. According to Livage & Henry[6] and Brinker,[7] with ortho esters a condensation via (2) should be the preferred reaction. Si—C-substituted esters show remarkable differences in reactivity compared to ortho esters,[8,9] suggesting that electronegativity considerations only are not sufficient to explain these differences.

Material Properties

The dried amo, diamo and triamo condensates are transparent and optically homogeneous. X-ray analysis shows the amorphous character

for all types and all acid concentrations. The densities range around 1·3 g cm^{-3}. The materials are soluble in water (they can be recast from this solvent) and are non-porous.

The thermal stability in air was determined by thermal and thermogravimetric analysis coupled with mass spectrometry. These measurements for amo with $CF_3SO_3H:N = 0{\cdot}035$ are shown in Fig. 6. The endothermic peak (a) around 140°C can be clearly attributed to the evaporation of adsorbed water, carbon dioxide and nitrogen dioxide as shown by mass spectroscopic analysis. The exotherm peak (b) at 260°C combined with the weight loss of about 9% corresponds mainly to the formation of H_2O, a weak CO_2 formation and a yet unknown amount of alkyl groupings by degradation. The H_2O evolution can be explained by further condensation based on the increasing network mobility with temperature increase. As known

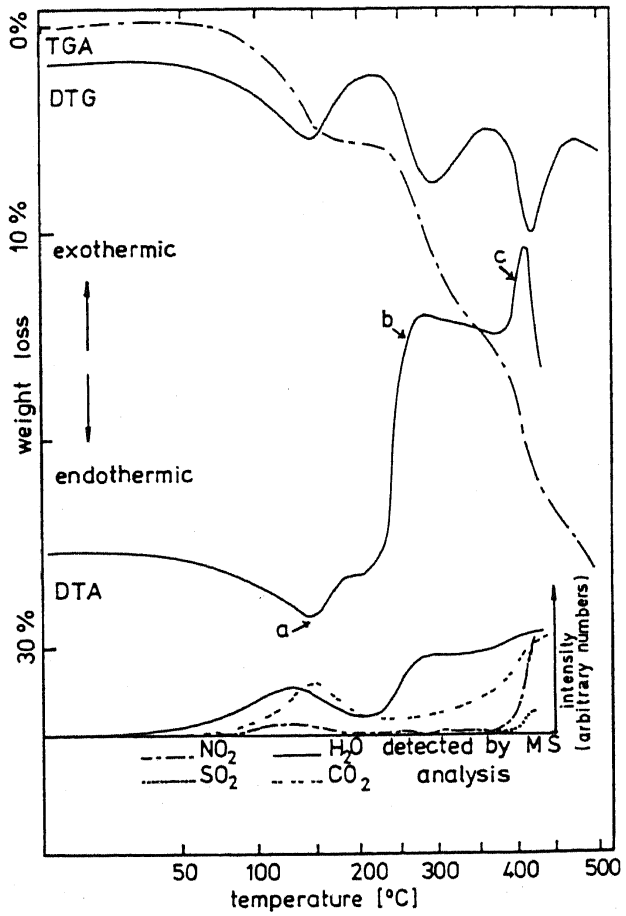

Figure 6. DTA, DTG, TGA and MS curves for amo 0·035 in air.

from IR investigations, after very long reaction times the ≡SiOH content in the condensates increases due to the steric hindrance-based slow down of the condensation rate. Considerable decomposition by oxidation only starts above 370°C (peak (c)). CO_2, H_2O and NO_2 are formed by oxidation of hydrocarbons and amines, SO_2 by reduction of CF_3SO_3H. Measurements carried out with diamo and triamo show the same phenomena and confirm a thermal stability of the materials at least up to 220°C.

Electrical Properties

The conductivity versus the reciprocal temperature exhibits non-Arrhenius behaviour in the 15–130°C range (Fig. 7) and it is

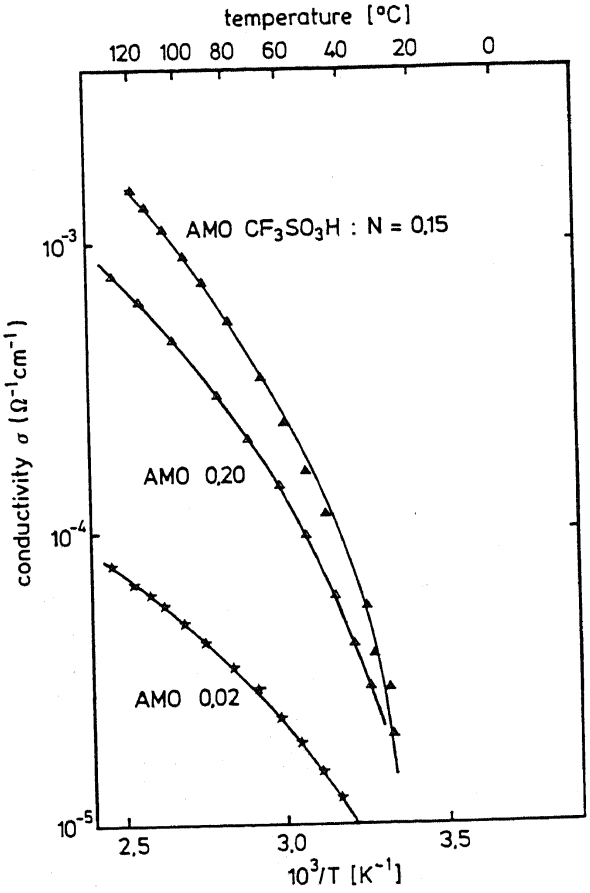

Figure 7. Log (conductivity) versus the $1/T$ plot of amo with different CF_3SO_3H contents.

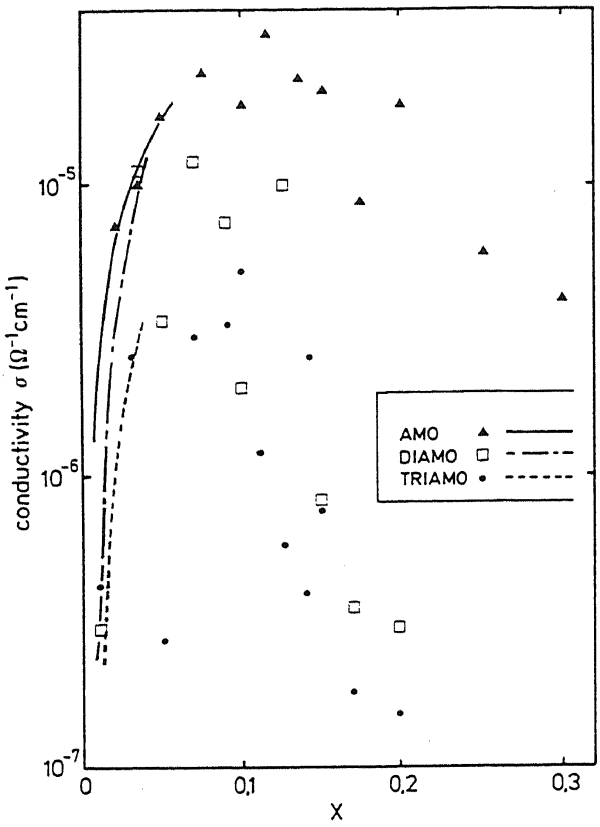

Figure 8. 25°C conductivities of amo, diamo and triamo with various ratios $x = CF_3SO_3H : N$.

characteristic for a free volume limited diffusion process, which can be expressed by the VFT (Vogel–Fulcher–Tamman) equation[10] (computer analysis yields the best-fit values for the parameters within this equation). The conductivity depends on the CF_3SO_3H concentration. It first increases with increasing acid concentration, but decreases between ratios of $CF_3SO_3H:N > 0{\cdot}15$ and $0{\cdot}20$. Undoped amo shows a conductivity of about $10^{-8}\,\Omega^{-1}\,cm^{-1}$ at room temperature. Figure 8 shows the room temperature conductivities of amo, diamo and triamo with different $CF_3SO_3H:N$ ratios x. The optimum for all three compounds lies around $x = 0{\cdot}1$ with a conductivity error of ±20% due to the scattering of the experimental data. The experiment also shows a slight difference in the observed conductivity maxima between the three types. To develop a structural model to explain this behaviour, more detailed investigations are necessary. The results for amo are

comparable to those of Charbouillot *et al.*[11] The best conductivity at room temperature is obtained with amo 0·115: $\sigma = 3{\cdot}3 \times 10^{-5}\ \Omega^{-1}\,cm^{-1}$. It corresponds to the following parameters of the VTF equation: −103°C for the ideal glass transition temperature and $9{\cdot}5 \times 10^{-2}$ eV for the pseudo-activation energy. According to Charbouillot,[3] the conductivity is due to the motion of the alkylamine chains, allowing an ion hopping mechanism.

As shown in Fig. 9(a) the cathodic wave corresponding to the evolution of hydrogen is stable:

$$H^+(\text{ORMOLYTE}) + e^-(\text{Pt}) \rightarrow \tfrac{1}{2}H_2 + \text{ORMOLYTE}$$

The anodic wave degrades the polymer and since the position of this peak is poorly defined, we have proceeded by gradually widening the studied domain. Between 0·0 V/Ref. and 1·0 V/Ref. the cyclic voltammogram is stable and the involved redox reactions do not affect the material (Fig. 9(b)). Over 1·2 V/Ref. the cycle is not stable and after

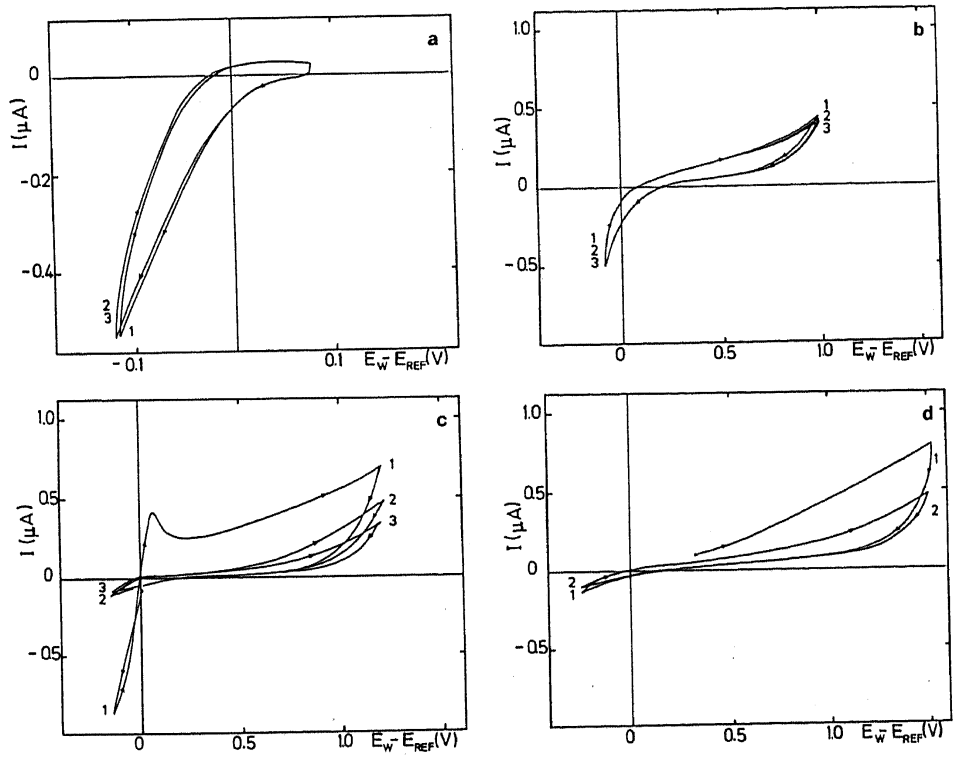

Figure 9(a–d). Cyclovoltammograms of amo 0·115. $dE/dt = 10$ mV/s, $T = 100$°C, vacuum.

the first cycle, the cathodic wall is suppressed (Fig. 9(c)). This fact can be attributed to the degradation of the alkylamine chains, probably leading to an insulating layer. This is confirmed by cycles starting on the anodic side, where no cathodic wall is observed (Fig. 9(d)). In Fig. 9(c) due to the more negative potential applied, there is an enhanced production of hydrogen, which will be oxidized first in the first cycle resulting in the maximum in this figure. The stability window was found for diamo and triamo systems equal to 1·2 V, too.

CONCLUSION

The sol–gel process offers possibilities of preparing new materials with specific properties. The electrolytes obtained by this route present interesting properties: amorphous structure at room temperature, transparency, temperature stability and ionic conductivity.

For application of these new materials as conductors, which are comparable to the best polymer ionic conductors, it is of general importance to know the influence of the starting compounds and important reaction parameters on the polycondensation process and the gel properties. The knowledge and the control of structure by a more thorough understanding of the hydrolysis and condensation reaction will allow synthesis of ion conducting materials with tailored properties based on ORMOCERs (ORganically MOdified CERamics).[12] Forseeable practical electrochemical applications are electrolytes in solid state batteries, membranes in low temperature fuel cells, electrochromic displays and windows and hydrogen sensors.[13]

REFERENCES

1. Defendini, F., Thesis, Institut National Polytechnique, Grenoble, 1987.
2. Ravaine, D., Seminel, A., Charbouillot, Y. & Vincens, M., *J. Non-Cryst. Solids,* **82** (1986) 210–19.
3. Charbouillot, Y., Thesis, Institut National Polytechnique, Grenoble, 1987.
4. Schmidt, H., *J. Non-Cryst. Solids,* **100** (1988) 51–64.
5. Plueddemann, Edwin P. In: *Silane Coupling Agents.* Plenum Press, New York and London, 1982.
6. Livage, J. & Henry, M. In: *Ultrastructure Processing of Advanced Ceramics 183–195,* ed. J. D. Mackenzie & D. R. Ulrich. John Wiley, New York, 1988.

7. Brinker, C. J., *J. Non-Cryst. Solids,* **100** (1988) 31–50.
8. Schmidt, H., Scholze, H. & Kaiser, A., *J. Non-Cryst. Solids,* **63** (1984) 1–11.
9. Voronkov, M. G., Mileshkevich, V. P. & Yuzhelevskii, Yu. A., *The Siloxane Bond.* Consultants Bureau, New York, 1978.
10. Ratner, Mark A. In: *Polymer Electrolyte Reviews 173–236.* Elsevier Applied Science, London and New York, 1987.
11. Charbouillot, Y., Ravaine, D., Armand, M. & Poinsignon, C., *J. Non-Cryst. Solids,* **108** (1988) 325–30.
12. Schmidt, H. In: *Inorganic and Organometallic Polymers.* ACS Symposium Series 369, 1988.
13. Popall, M. & Schmidt, H. In: TEC 88, Grenoble, Materiaux. Proceedings (in press).
14. Orcel, G., Phalippou, J. & Hench, L. L., *J. Non-Cryst. Solids,* **88** (1986) 114–30.